Variations in Grain Boundary Segregation for Nanocrystalline Stability and Strength

By

Oscar Figueroa III

Submitted to the Department of Material Science and Engineering

on May 4th, 2012

in partial fulfillment of the Requirements for the Degree of

Bachelor of Science

Signature of Author.....

Department of Materials Science and Engineering

May 4, 2012

Certified by.....

Christopher Schuh

Department Head, Material Science and Engineering

Thesis Supervisor

Accepted by.....

Jeffery Grossman

Professor of Materials Science and Engineering

Chair, Undergraduate Committee

Variations in Grain Boundary Segregation for Nanocrystalline Stability and Strength

By

Oscar Figueroa III

Submitted to the Department of Material Science and Engineering

on April 27, 2012

in partial fulfillment of the Requirements for the Degree of

Bachelor of Science

Abstract

In the last few decades, nanocrystalline metals have been of increasing interest. Their ability to show increased yield strength and uniform structure show them to be potentially useful in many applications. Additionally, nanocrystalline metals have become more easily manufactured in recent years, allowing for more testing and more use within industrial settings. However, nanocrystalline metals are still highly unstable, mainly due to temperature related growth. Grain boundary segregation is one way in which materials can keep nano length-scale grains. This process involves metal alloys that preferentially segregate the alloying material to the grain boundaries, potentially leading to Grain Boundary Embrittlement (GBE). Using an ideal work of fracture equation, $\gamma = 2\sigma_s - \sigma_g$, the energy required to fracture nanocrystalline metal alloys was obtained, and predicted grain stability. Fracture toughness data is also calculated and compared. A contrast between bulk and nanocrystalline alloys is then made, showing benefits to the use of either set of materials for specific alloy functions.

Thesis Supervisors: Christopher Schuh, Heather Murdoch

Title: Department Head of Material Science and Engineering, Graduate Student

Table of Contents

List of Tables:

List of Figures:

Introduction

1.1 Background

Stabilization of nanocrystalline metals has always been a limiting factor for their production. Their small grain sizes lead to grain growth in order to satisfy energy minimization, leading to an inherent instability within the material. However, this class of materials has many uses. Due to the difference in the ratio of grain and grain boundary between bulk and nanocrystalline metals, differences in properties are also observed. Because these alloys have grains smaller than average, bulk materials, grain boundary properties play a larger role in global material characteristics. However, the greater surface area of grains in nanocrystalline alloys allows for Grain Boundary Segregation (GBS). GBS is a mechanism by which one constituent of an alloyed material preferentially collects near grain boundaries. This effect helps to lower the overall free energy of the system. Work has been done to show a model which can be used to predict stabilization content of nanocrystalline metal alloys in which segregation is a dominate process. Using a Regular Nanocrystalline Solution (RNS) model developed by Trelewicz and Schuh describing grain boundary surface segregation, research was done to both broaden the scope of previous work, and expand upon characterization of nanocrystalline alloys *(Trelewicz and Schuh)*. The RNS model was used for a set of alloys to determine stability, taking advantage of a simple surface energy model by Weissmuller.

$$\gamma = \gamma_0 - \Gamma(\Delta H\_seg + kT\ ln\ X)v^{-} \qquad (1)\ \text{(Weissmuller)}$$

Segregation can be due to many factors, including size mismatch of alloying elements and differences in surface energy. Regardless the cause, a non-homogeneous material within and between grains is created, and can potentially lead to Grain Boundary Embrittlement (GBE). GBE is a phenomenon which causes grain boundaries to become brittle, especially compared to the bulk material. Embrittlement leads to a less elastic material response, which now shows a different deformation mechanism characterized namely by fracture. These materials, while able to take on higher loads, are less able to deform under stress. But, higher yield strength can make materials desirable. Many applications require stiff, unyielding products. Grain Boundary Segregation is required for stabilizing nanostructure materials; however, it may cause GBE. In some cases, this may be an acceptable byproduct as with products with high loading. In other cases, this could be a detriment, as NC materials are already less plastic than their larger grained counterparts. These mechanisms can work together with small grains to create a material capable of very high yield strength.

In the work detailed by Trelewicz and Schuh, a new model for a regular nanocrystalline solution was created for looking at the free energy of grains on the nanometer level *(Trelewicz and Schuh)*. This model takes the "intergranular" and "bulk" components of grains separately in addition to a regime called the "transitional" region.

This is done so that all energy components can be considered. Each section has its own characteristics; *Figure 1* below shows a nanocrystalline grain under the RNS model.

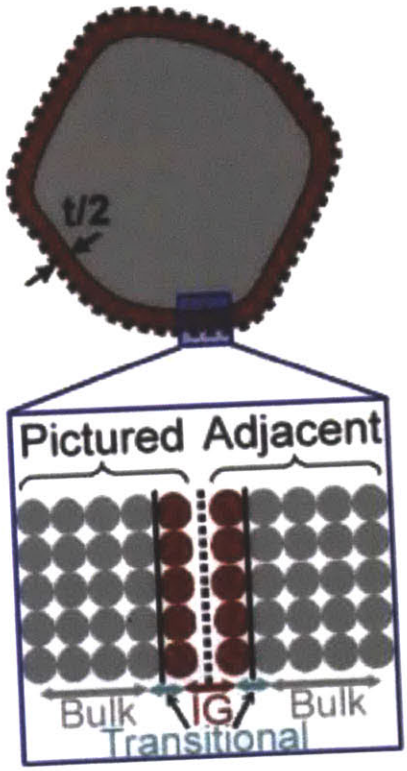

Figure 1: RNS model of grains depicting the three granular regions.(Trelewicz and Schuh)

The red regions specify the intergranular sections, IG, and the grey regions indicate Bulk material, B. The black, solid line separating the red and grey is the transitional region, which shares characteristics from both bulk and intergranular. As is indicated in the figure above, the transitional section of the grain doesn't contain whole atoms, but is instead used to understand a distinction in energy due to bonding characteristics which differ between the bulk and intergranular regions.

Using this representation, a different solution energy is achieved

$$U_{soln} = \sum_r \{N_r^{AA} E_r^{AA} + N_r^{BB} E_r^{BB} + N_r^{AB} E_r^{AB}\} \quad (2)$$

which takes all three regions into consideration. Here, r represents the region being summed over; either bulk, intergranular, or transitional. A standard approach is then taken, finding a solution energy of mixing

$$U_{mix} = U_{soln} - U_{ref} \quad (3)$$

where U_{ref} defines a reference of an ideal, interface-free solution of the same composition. U_{ref} is defined as

$$U_{ref} = \frac{zN^A}{2} E_b^{AA} + \frac{zN^B}{2} E_b^{BB} \quad (4)$$

with z as the coordination number, N as the number of bonds, and E as the energy per bond. Simplifying these equations, and inserting them into a full free energy expression, the following equation is derived for the grain boundary energy in a nanocrystalline grain

$$\gamma = \gamma_A - \frac{ztX_{ig}}{\Omega}\left[\omega_b - \omega_{ig}\left(1 - \frac{\nu}{1-f_{ig}}\right) - \frac{\Omega}{zt}(\gamma_B - \gamma_A)\left(1 - \frac{\nu}{1-f_{ig}}\right)\right] - \frac{zt}{\Omega}\left[(X_b{}^2 - 2X_bX_{ig})\omega_b + X_b{}^2\omega_b\left(1 - \frac{\nu}{1-f_{ig}}\right)\right] + \frac{zt\nu}{\Omega(1-f_{ig})}\left[\{X_{ig}(X_{ig} - X_b) + X_b(1 - X_{ig})\}\omega_{ig} + X_b\frac{\Omega}{zt}(\gamma_B - \gamma_A)\right] + \frac{tKT}{\Omega}\left[X_{ig}\ln\left(\frac{X_{ig}}{X_b}\right) + (1 - X_{ig})\ln\left(\frac{1-X_{ig}}{1-X_b}\right)\right] \quad (5)\ (\text{Weissmuller})$$

In this equation, γ is the total grain boundary energy, z is the coordination number, t is the inter-granular shell thickness, X is the percent alloying material (in each of the two regions ig and b), Ω is solvent atomic volume, ν is the transitional bond fraction, representing the effective coordination for atoms contributing bonds to the transitional bonding region (taken to be ½), and f_{ig} the intergranular volume fraction and related to the grain size and grain boundary thickness by

$$f_{ig} = 1 - (\frac{d-t}{d})^D \quad (6)$$

In addition, K represents the Boltzmann constant, T represents temperature in Kelvin, and ω represents a difference in bond energies between alloying constituents

$$\omega_r = \left(E_r^{AB} - \frac{E_r^{AA} - E_r^{BB}}{2}\right) \quad (7) \textit{ (Trelewicz and Schuh)}$$

where r again stands for either the "bulk", "intergranular", or "transitional" sections of the grain. For the above variables, A and B represent alloying elements, and ig, t, and b represent "intergranular", "transitional", and "bulk" portions of individual grains. Most of these parameter are readily available for binary systems while other methods can be used to connect properties to parameters.

This work tries to shed some light on what types of solute segregation states are required for stabilization in nanocrystalline alloys, and how this will affect grain boundary embrittlement.

1.2 Problem Statement

As previously stated, there is still much to learn about nanocrystalline metals. Characterization and stability are two key features which people want and need to know more about before many widespread applications can be implemented. But how can results be found? My research was aimed at the use of simulation and experimental data to show how characterization and stability of nanocrystalline metal alloys can be determined.

Using the work RNS model, work was carried out to expand and determine measurable material characteristics. In "Grain boundary segregation and thermodynamically stable binary nanocrystalline alloys", a new way to describe the grain boundary energy in segregated system derived *(Trelewicz and Schuh)*. Combining this equation with simple models to calculate surface energy and the work of fracture, a prediction can be made about the possibility of grain boundary embrittlement. The work of fracture equation being used defines an ideal situation in which a non-segregated material is undergoing fracture.

$$\gamma = 2\sigma_s - \sigma_g \qquad (8)$$

Here, σ_g is the grain boundary energy, σ_s is the surface energy, and γ is the work of fracture. The factor of two is included to describe the ideal creation of two new surfaces in the material upon fracture. While this equation does not exactly replicate the grains under the assumptions being made, it is a close approximation. The biggest discrepancy comes from the grains being segregated, which this equation

does not account for. σ_g can be attained from the RNS model, while the first part of my work focused on attaining σ_s. The model used for surface energy was a simple weighting of constituents. For example, an alloy of 5% Ni with 95% Fe would have a total surface energy of 5% that of Ni plus 95% that of Fe. For the purposes of this study, a simple approximation seemed sufficient, and can be replaced in the future for higher precision and accuracy.

Knowing these equations, both stabilization and fracture characteristics can be acquired. Stabilization can be determined from grain boundary energy minimization values of zero, and fracture energy can be compared with experimental data. Additionally, cases with less than complete stability can also be analyzed, such that a percentage of grain boundary energy is reduced from a pure scenario. While actual numbers cannot be trusted with confidence due to the number of assumptions, trends can and do appear, which have a reasonable degree of certainty.

Methodology

2.1 Procedures for calculating alloy stabilization and strength

Taking the equation 5 derived by Trelewicz and Schuh, a minimum in free energy can be found for grain boundaries by reducing the grain boundary energy to zero. The equation may look daunting, but it is capable of solving for grain boundary energies without using experimentally unobtainable quantities. While the ω terms can be difficult to acquire, they are crucial to understanding grains in this new model. Other values can be predetermined. The grain boundary thickness is approximated to 0.5 nm (Fultz and Frase).Grain sizes can be adjusted and estimated based on our desired material granular dimensions. D can be taken as 3 to describe the three-dimensional grains, and ν can be taken to 0.5, giving a 50% chance of transitional bonds being assigned to either the bulk, or grain boundary. Finally, temperature, T, can be chosen such that testing and use of the material would be feasible.

Plotting γ versus X_{ig} shows how grain boundary energy varies with solute content. This allows compositions to be determined which will be stable at a given. However, this requires surface energies for individual elements being alloyed, as well as heat of mixing data. Both these sets of values were acquired for almost 200 distinct elements and crystal orientations, and were incorporated into grain boundary energy calculations, keeping crystal structures in mind (Ibach and Sander). *Table 1* below is a representative sample of surface energy values used in stability

calculations. These values were compiled into several defining lists, and then separated by compatibility of alloying elements and crystal structures. *Table 2* below shows a more valuable set of data, separating alloys into more compatible arrays. The surface energy value for their alloys was then calculated. Again, a simple surface energy model was used for convenience of calculations. It was determined that for initial work, an additive model would be sufficient in order to flesh out general trends within the nanocrystalline metal alloys.

Material, plane		Alloy	Ac(100), fcc	Ac(110), fcc	Ac(111), fcc	Ag(100)
	S.E. J/m^2		0.732	0.681	0.868	1.2
Alloy			0.72834	0.677595	0.86366	1.194
Ac(100), fcc	0.732	0.00366	0.732	0.681255	0.86732	1.19766
Ac(110), fcc	0.681	0.00341	0.731745	0.681	0.867065	1.19741
Ac(111), fcc	0.868	0.00434	0.73268	0.681935	0.868	1.19834
Ag(100)	1.2	0.006	0.73434	0.683595	0.86966	1.2
Ag(110), fcc	1.238	0.00619	0.73453	0.683785	0.86985	1.20019
Ag(111)	0.62	0.0031	0.73144	0.680695	0.86676	1.1971
Al(100), fcc	1.347	0.00674	0.735075	0.68433	0.870395	1.20074
Al(110), fcc	0.912	0.00456	0.7329	0.682155	0.86822	1.19856
Al(110), bcc	1.03	0.00515	0.73349	0.682745	0.86881	1.19915
Al(111)	0.96	0.0048	0.73314	0.682395	0.86846	1.1988
Au(100)	1.627	0.00814	0.736475	0.68573	0.871795	1.20214
Au(110), fcc	1.7	0.0085	0.73684	0.686095	0.87216	1.2025
Au(111)	1.248	0.00624	0.73458	0.683835	0.8699	1.20024
Ba(100), bcc	0.353	0.00177	0.730105	0.67936	0.865425	1.19577
Ba(110), bcc	0.376	0.00188	0.73022	0.679475	0.86554	1.19588
Ba(111), bcc	0.397	0.00199	0.730325	0.67958	0.865645	1.19599

Table 1: Representative array of surface energies.

Material, plane		Alloy	Ac(100), fcc	Ag(100)	Al(100), fcc	Au(100)	Ca(100), fcc
	S.E. J/m^2		0.732	1.2	1.347	1.627	0.542
Alloy			67064.6542	109942	123409.958	149063.104	49657.162
Ac(100), fcc	0.732	3529.72	70594.3728	113472	126939.677	152592.823	53186.8806
Ag(100)	1.2	5786.42	72851.0782	115728	129196.382	154849.528	55443.586
Al(100), fcc	1.347	6495.26	73559.9151	116437	129905.219	155558.365	56152.4229
Au(100)	1.627	7845.43	74910.0807	117787	131255.385	156908.531	57502.5885
Ca(100), fcc	0.542	2613.53	69678.189	112556	126023.493	151676.639	52270.6968
Cu(100)	2.166	10444.5	77509.1495	120386	133854.453	159507.599	60101.6573
Ir(100)	3.722	17947.6	85012.2126	127890	141357.516	167010.662	67604.7204
Nb(100), fcc	1.956	9431.87	76496.5253	119374	132841.829	158494.975	59089.0331
Ni(100)	2.426	11698.2	78762.8747	121640	135108.179	160761.325	61355.3825
Pb(100), fcc	0.377	1817.9	68882.5557	111760	125227.86	150881.006	51475.0635
Pd(100)	2.326	11216	78280.6727	121158	134625.977	160279.123	60873.1805
Pt(100)	2.734	13183.4	80248.0569	123125	136593.361	162246.507	62840.5647
Rh(100)	2.799	13496.8	80561.4882	123439	136906.792	162559.938	63153.996
Sr(100), fcc	0.408	1967.38	69032.0384	111909	125377.342	151030.488	51624.5462
Tc(100), fcc	3.83	18468.3	85532.9908	128410	141878.295	167531.441	68125.4986
Th(100), fcc	1.468	7078.73	74143.3796	117021	130488.683	156141.829	56735.8874
Yb(100), fcc	0.478	2304.93	69369.5798	112247	125714.884	151368.03	51962.0876

Table 2: Compiled array of surface energy values base on crystallographic orientation.

Surface energies were computed for a range of compositions, from 0.5at% to 8at% alloying material. This array was assumed to be of adequate range due to the lack of intermetallics which could possibly occur. In addition, looking at 0.5% - 8% alloying materials shows the effects of dilute alloy composition, and whether stabilization can arise at low concentration. Considerable time was taken to organize these values into a meaningful array, at which point combinations of alloys for testing began. Selected alloys were then used in calculating the grain boundary energy using the RNS model. Once both of these values were determined, a work of fracture was also calculated. For this, another simplified model was used. Equation 8 was first derived by McLean, and describes an ideal work of fracture for a grain boundary with no segregation. And while segregation is indeed a factor within the constraints being considered in this study, the McLean model gives an idea of magnitude, and allows for reasonable accuracy for work of fracture data.

After material data was obtained, these models were used to find minimums in grain boundary energy and determine work of fracture data. This was done computationally, and led to some interesting data results.

Simulation Results

3.1 Material Stability Characterization

After running several sets of calculations, grain boundary energy data was attained. The energy, plotted against grain boundary composition, revealed several systems which may and may not show stability under the set of assumptions. Below is a table which signifies alloys considered for this study. Values are organized by segregation and mixing energies. This is done in an attempt to examine stability in terms of both values, as well as their combined influence.

	Positive Heat of Segregation	Heat of Mixing		Negative Heat of Segregation	Heat of Mixing
CuBi	$96000\ \frac{J}{m^2}$	$78100\ \frac{J}{m^2}$	**FeZn**	$-20000\ \frac{J}{m^2}$	$10600\ \frac{J}{m^2}$
NiZn	$23400\ \frac{J}{m^2}$	$56900\ \frac{J}{m^2}$	**NiCu**	$-7690\ \frac{J}{m^2}$	$14000\ \frac{J}{m^2}$
TaW	$13200\ \frac{J}{m^2}$	$20500\ \frac{J}{m^2}$	**FeCr**	$-1680\ \frac{J}{m^2}$	$-5\ 920\ \frac{J}{m^2}$
NiPb	$10700\ \frac{J}{m^2}$	$59000\ \frac{J}{m^2}$			

Table 3: A table representing alloys considered for stability. Organized by positive vs. negative Heat of Segregation, and from largest to smallest.

	Heat of Segregation	**Positive Heat of Mixing**		Heat of Segregation	**Negative Heat of Mixing**
CuBi	$96000\ \frac{J}{m^2}$	$78100\ \frac{J}{m^2}$	**FeCr**	$-1680\ \frac{J}{m^2}$	$-5\,920\ \frac{J}{m^2}$
NiPb	$10700\ \frac{J}{m^2}$	$59000\ \frac{J}{m^2}$			
NiZn	$23400\ \frac{J}{m^2}$	$56900\ \frac{J}{m^2}$			
TaW	$13200\ \frac{J}{m^2}$	$20500\ \frac{J}{m^2}$			
NiCu	$-7690\ \frac{J}{m^2}$	$14000\ \frac{J}{m^2}$			
FeZn	$-20000\ \frac{J}{m^2}$	$10600\ \frac{J}{m^2}$			

Table 4: A table representing alloys considered for stability. Organized by positive vs. negative Heat of mixing, and from largest to smallest.

Looking at CuBi, an alloy used in lead-free soldering applications, nanocrystalline segregation appears to occur. Segregation of either bulk or minority constituents towards the grain boundary is observed at different global compositions for two grain sizes. The figures below shows energy versus composition for a range of compositions. For reference, temperature is set at 300 Kelvin, and stability is measured for grain sizes of 12 nanometers, and 25 nanometers for all samples.

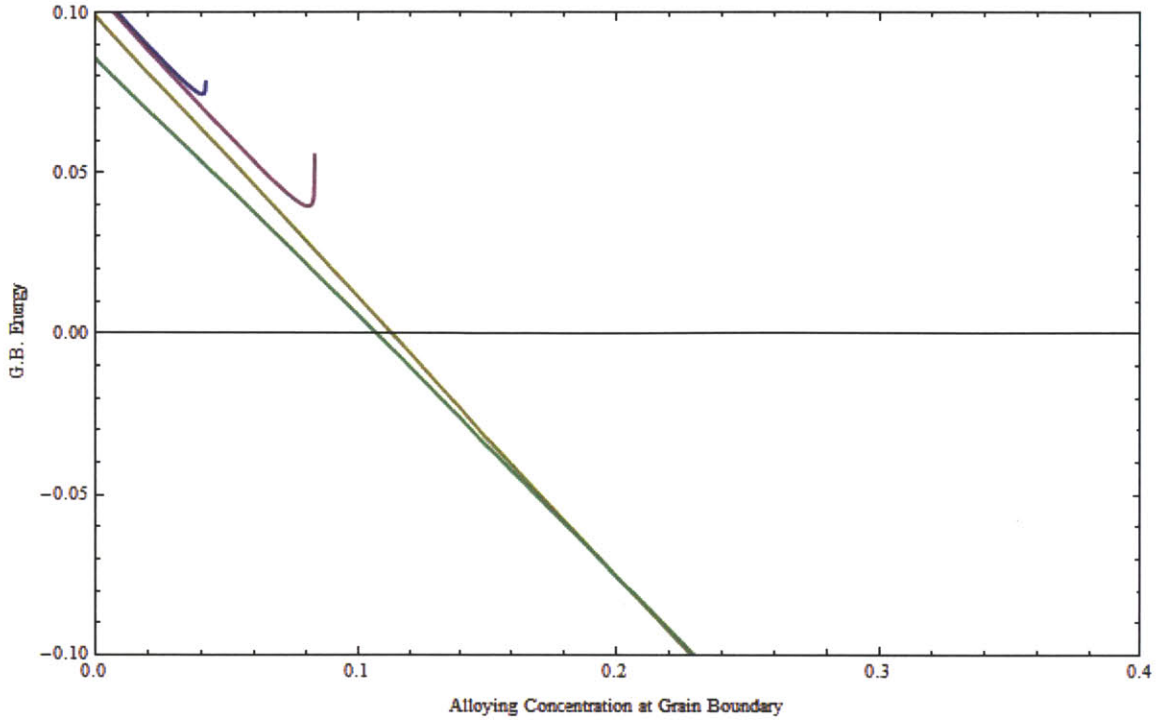

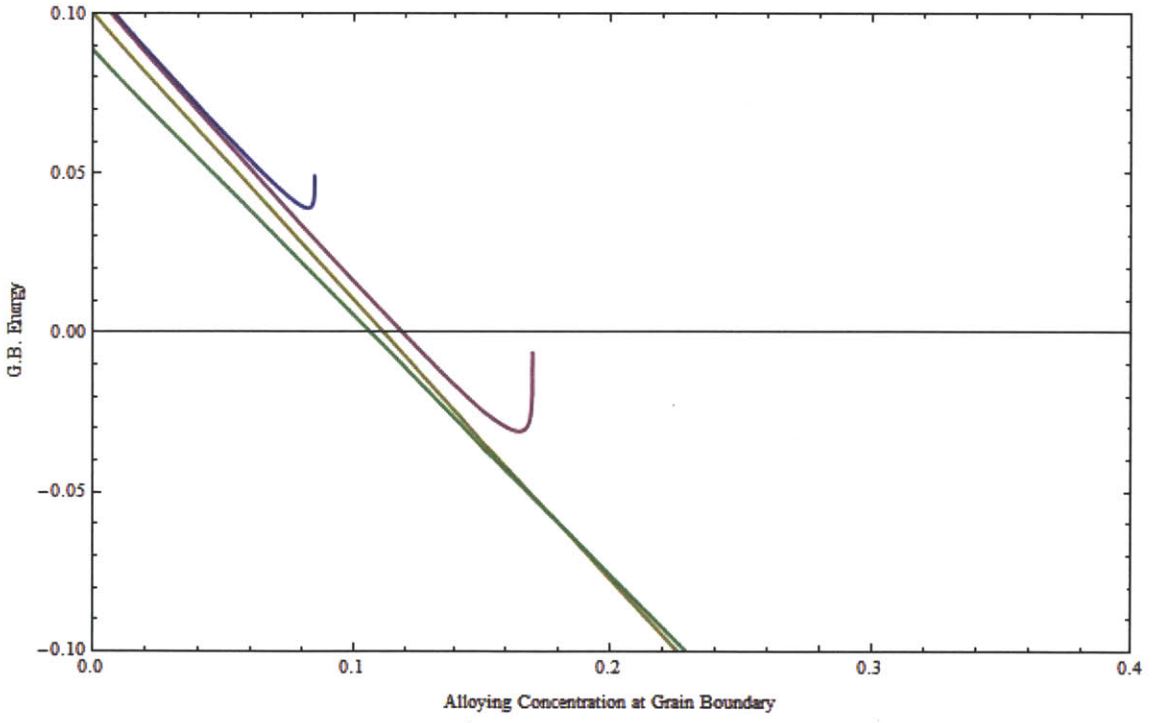

Figure 2: Grain Boundary energies in eV/ atom versus Grain Boundary Composition for CuBi samples. Blue:Cu0.5at%Bi,Purple:Cu1at%Bi,Yellow:Cu4at%Bi,Green:Cu8at%Bi. Top: D=12. Bottom: D=25.

As can be seen from looking at these graphs, lower grain boundary concentrations of Bi result in no segregation, while higher grain boundary concentrations show segregations characteristics. Both grain size shows segregation for a limited range.

FeCr shows a different trend: FeCr does not segregate for any compositions analyzed. The RNS model shows this alloy to display no tendency to segregate for either grain size.

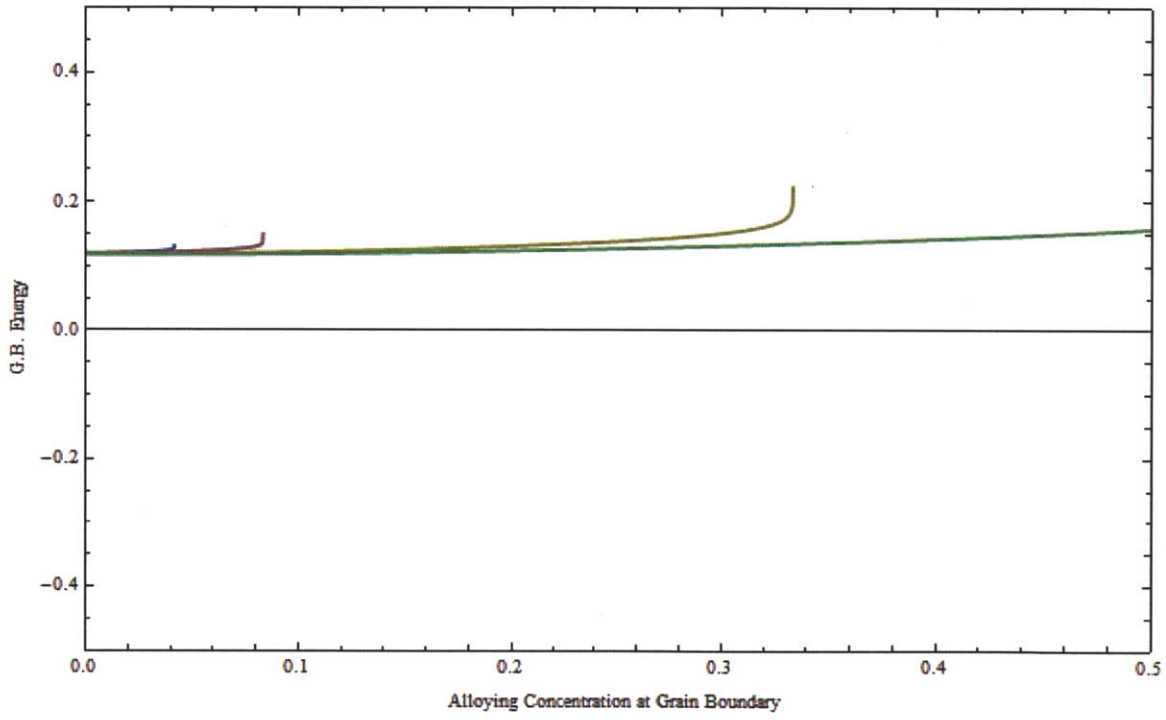

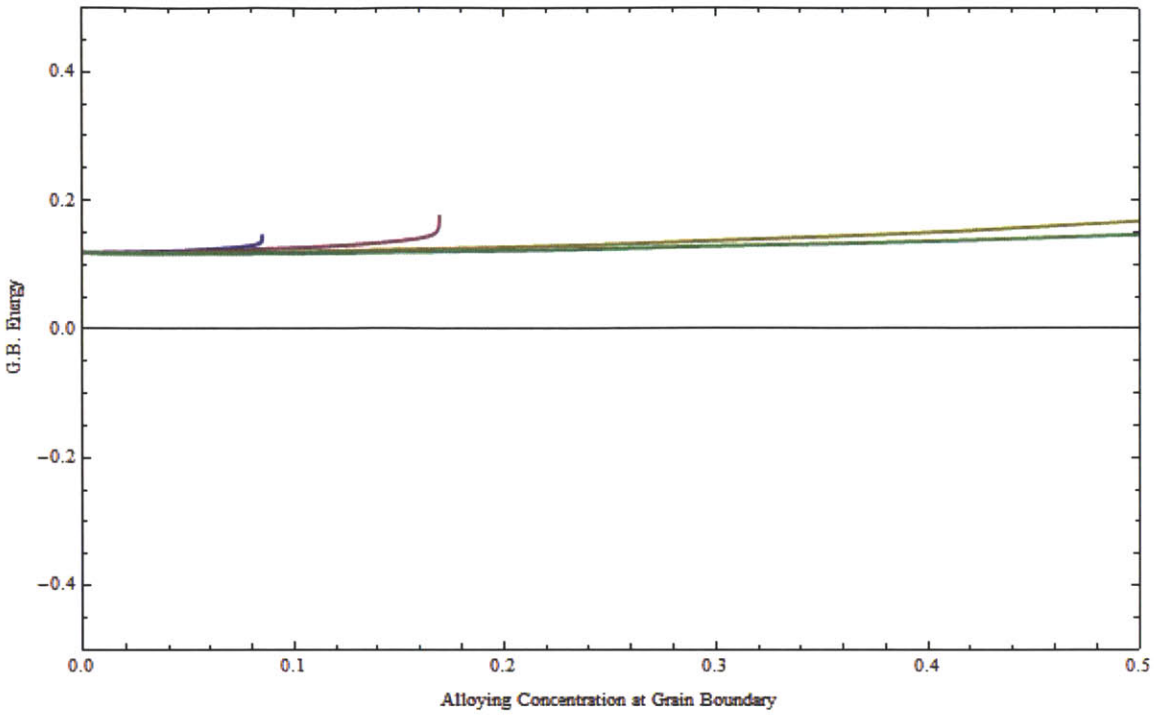

Figure 3: Grain Boundary energies in eV/ atom versus Grain Boundary Composition for FeCr samples. Blue:Fe0.5at%Cr,Purple:Fe1at%Cr,Yellow:Fe4at%Cr,Green:Fe8at%Cr. Top: D=12. Bottom: D=25.

Grains of FeCr are not expected to segregate in nanocrystalline alloys based on the information provided by these graphs.

FeZn shows a similar development for grain boundary energy vs. alloying concentration. Like FrCr, FeZn shows no propensity towards segregation within the grains. However, unlike FeCr, FeZn shows a higher propensity for segregation possible at higher concentrations/grain sizes.

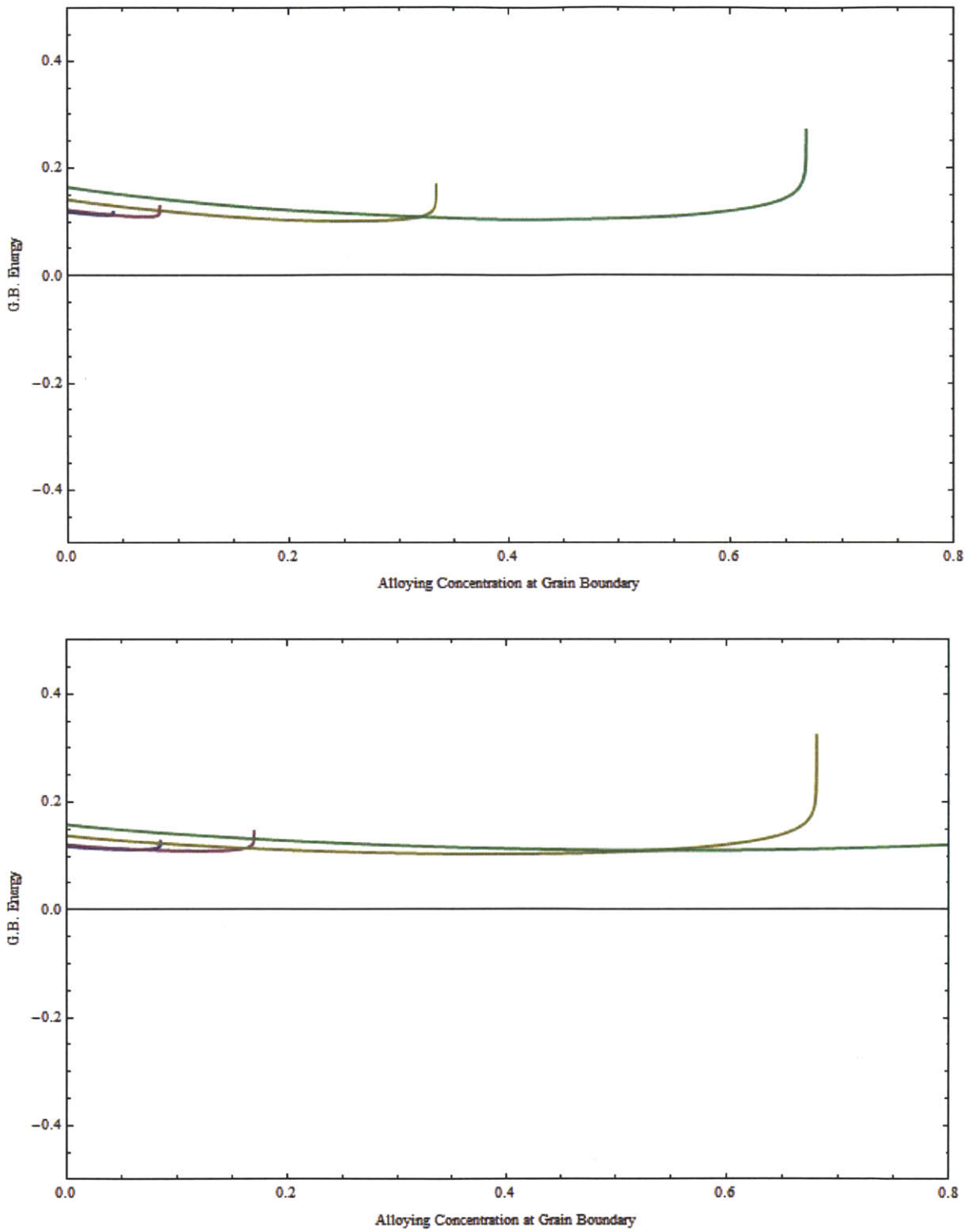

Figure 4: Grain Boundary energies in eV/ atom versus Grain Boundary Composition for FeZn samples. Blue:Fe0.5at%Zn,Purple:Fe1at%Zn,Yellow:Fe4at%Zn,Green:Fe8at%Zn. Top: D=12. Bottom: D=25.

These non segregating trends are seen for all concentrations, and for both grain sizes used for calculations.

NiCu is similar to FeZn in terms of segregation inclination. The major difference is that NiCu trends away from zero grain boundary energy, while FeZn trends towards zero. Grain boundary vs. concentration data is also similar in that all compositions at both grain sizes lie strictly above zero grain boundary energy.

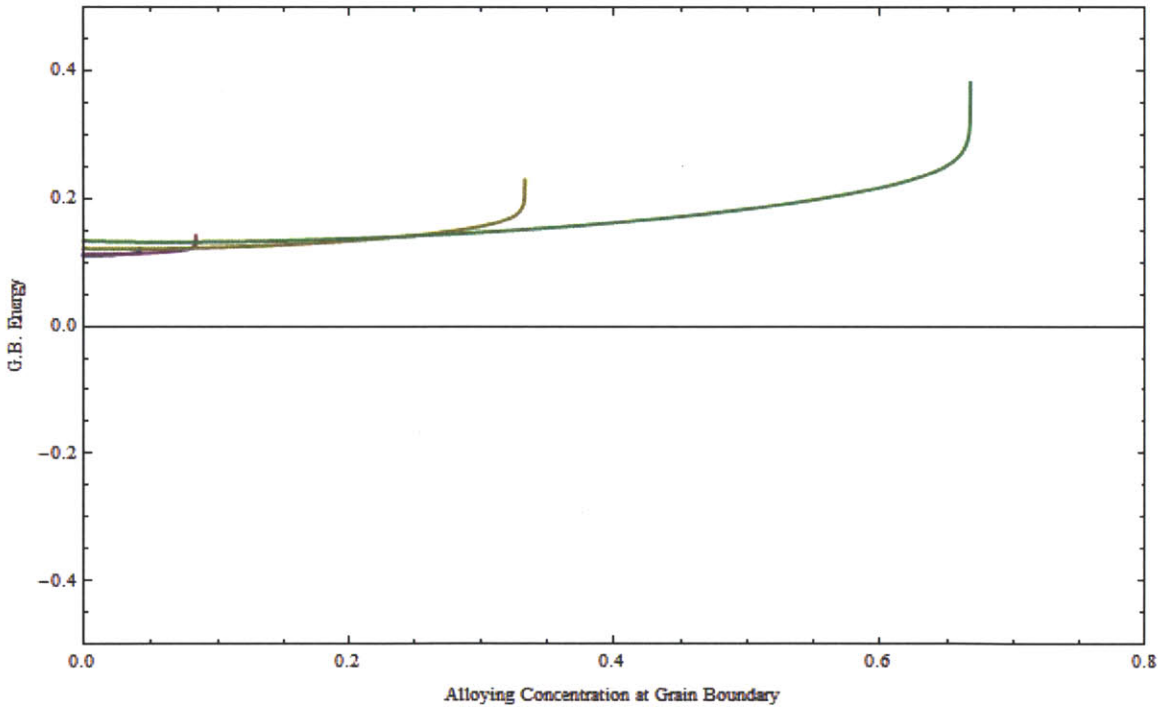

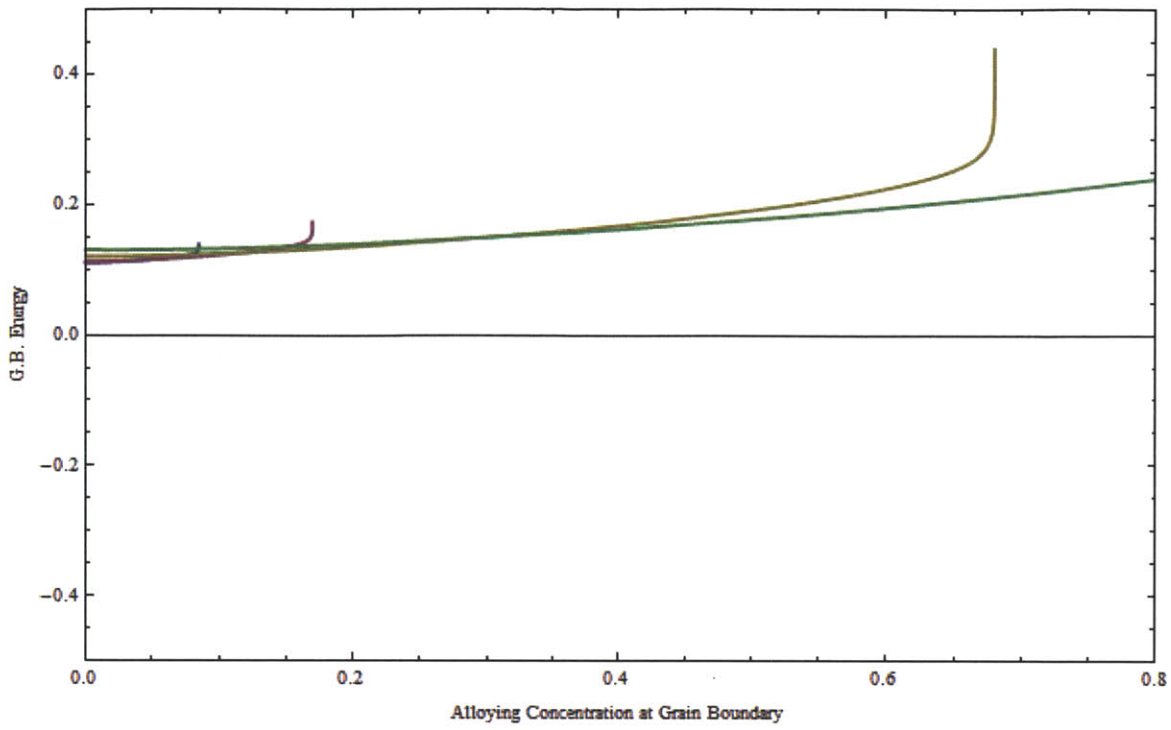

Figure 5: Grain Boundary energies in eV/ atom versus Grain Boundary Composition for NiCu samples. Blue:Ni0.5at%Cu,Purple:Ni1at%Cu,Yellow:Ni4at%Cu,Green:Ni8at%Cu. Top: D=12. Bottom: D=25.

As can be seen from the graphs, no segregation is assumed to occur in any of the NiCu samples studied in this work.

NiPb is similar to FeZn as well. No segregation is observed, but energy curves do appear to trend towards zero grain boundary energy concentrations.

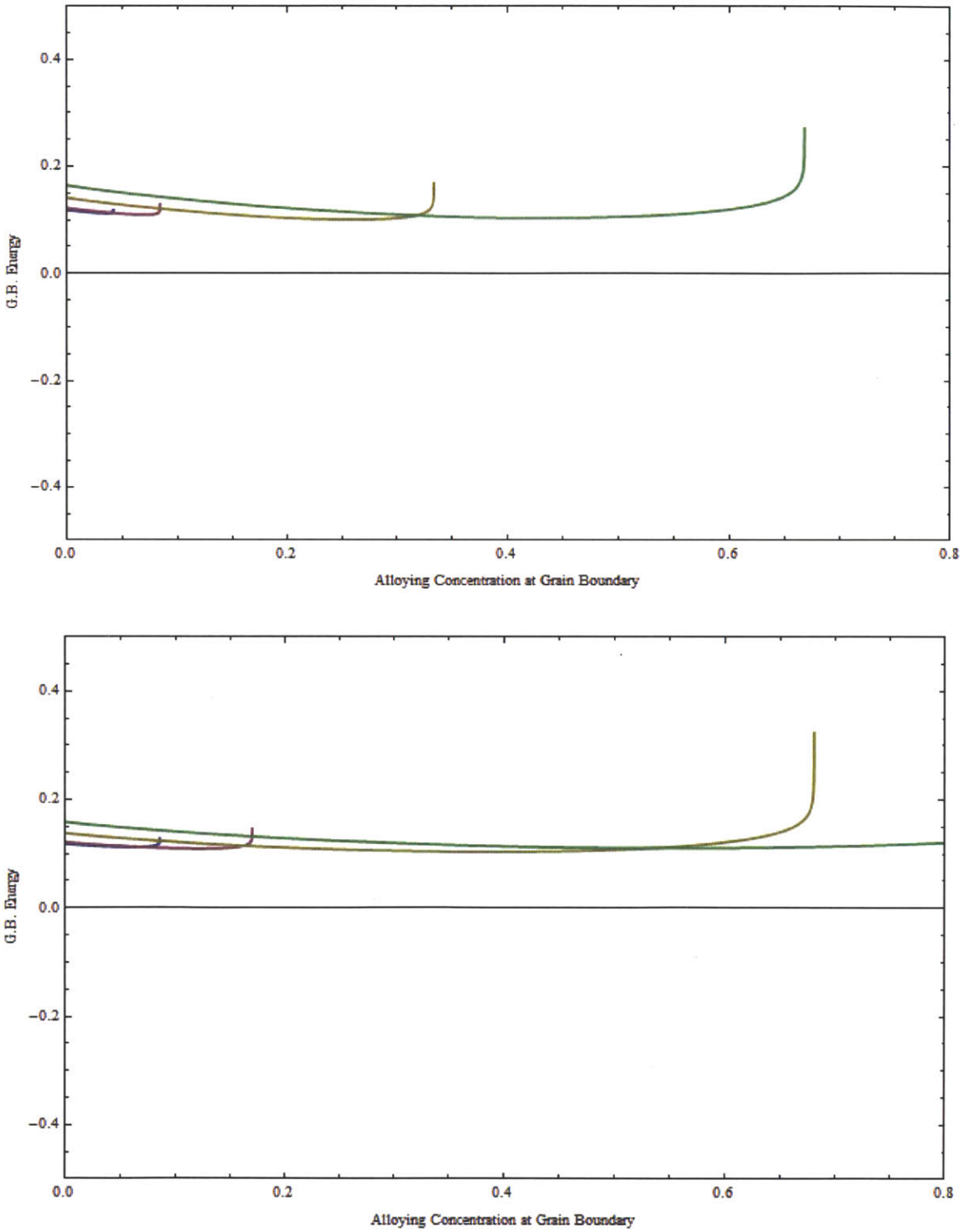

Figure 6: Grain Boundary energies in eV/ atom versus Grain Boundary Composition for NiPb samples. Blue:Ni0.5at%Pb,Purple:Ni1at%Pb,Yellow:Ni4at%Pb,Green:Ni8at%Pb. Top: D=12. Bottom: D=25.

NiPb shows no segregation propensity at all grain sizes, and for concentrations evaluated.

NiZn develops segregation behavior according to graphs of grain boundary energy vs. local grain boundary concentration. The main difference between CuBi and NiZn is that at low concentrations, no segregation concentration is seen in NiZn. While the Zn concentration increases at the boundaries, grains begin to show segregation compositions per global concentration value.

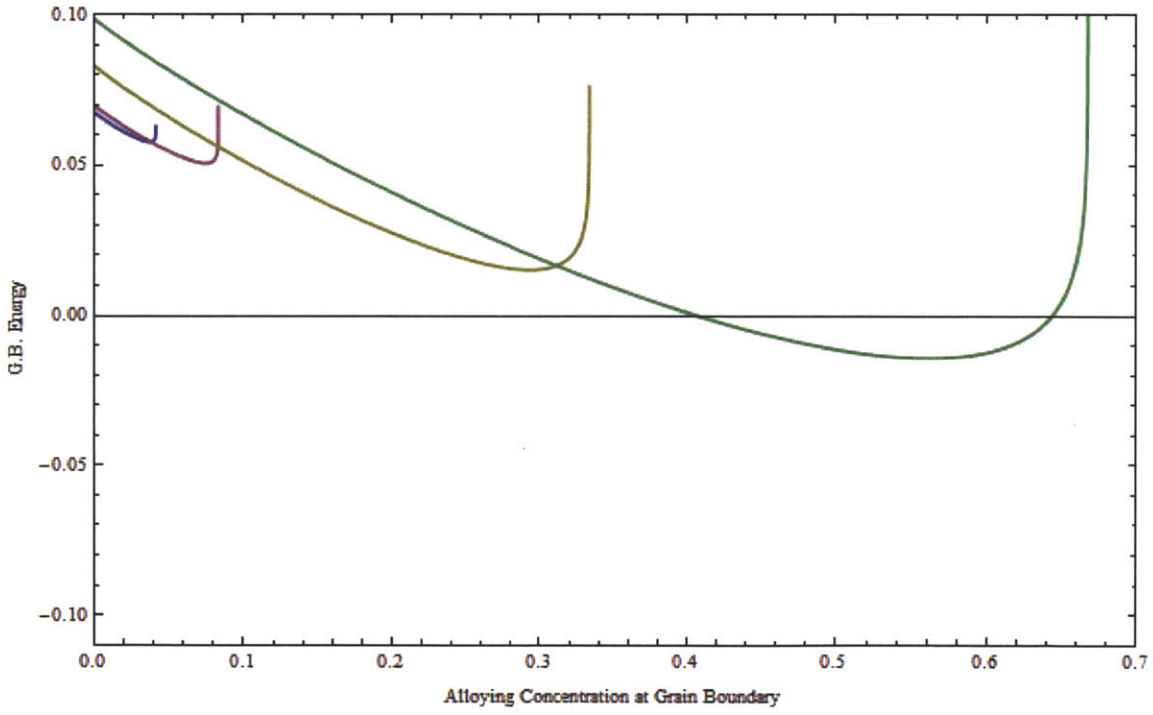

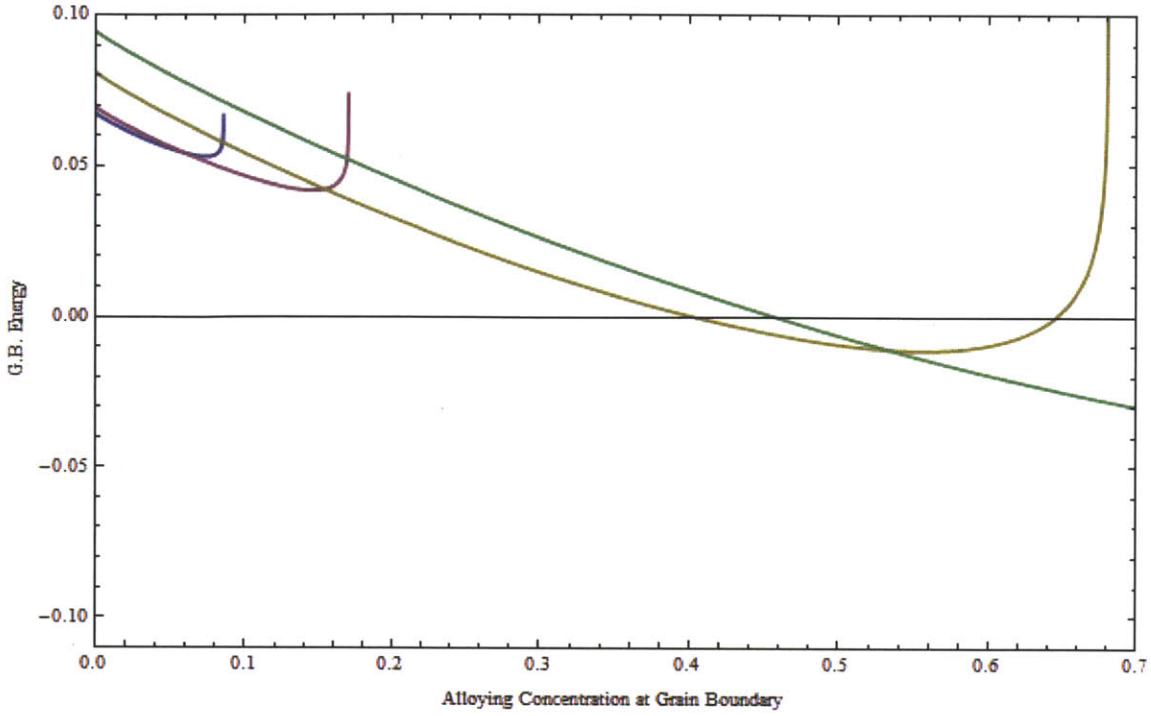

Figure 7: Grain Boundary energies in eV/ atom versus Grain Boundary Composition for NiZn samples. Blue:Ni0.5at%Zn,Purple:Ni1at%Zn,Yellow:Ni4at%Zn,Green:Ni8at%Zn. Top: D=12. Bottom: D=25.

The above figures also show how the curve is trending towards higher segregation compositions at higher global alloying compositions.

In the case of TaW, we see the same sorts of non-segregating trends again. TaW has no segregation concentrations per global composition, and has no tendency to display higher segregation concentrations with increasing global alloying composition.

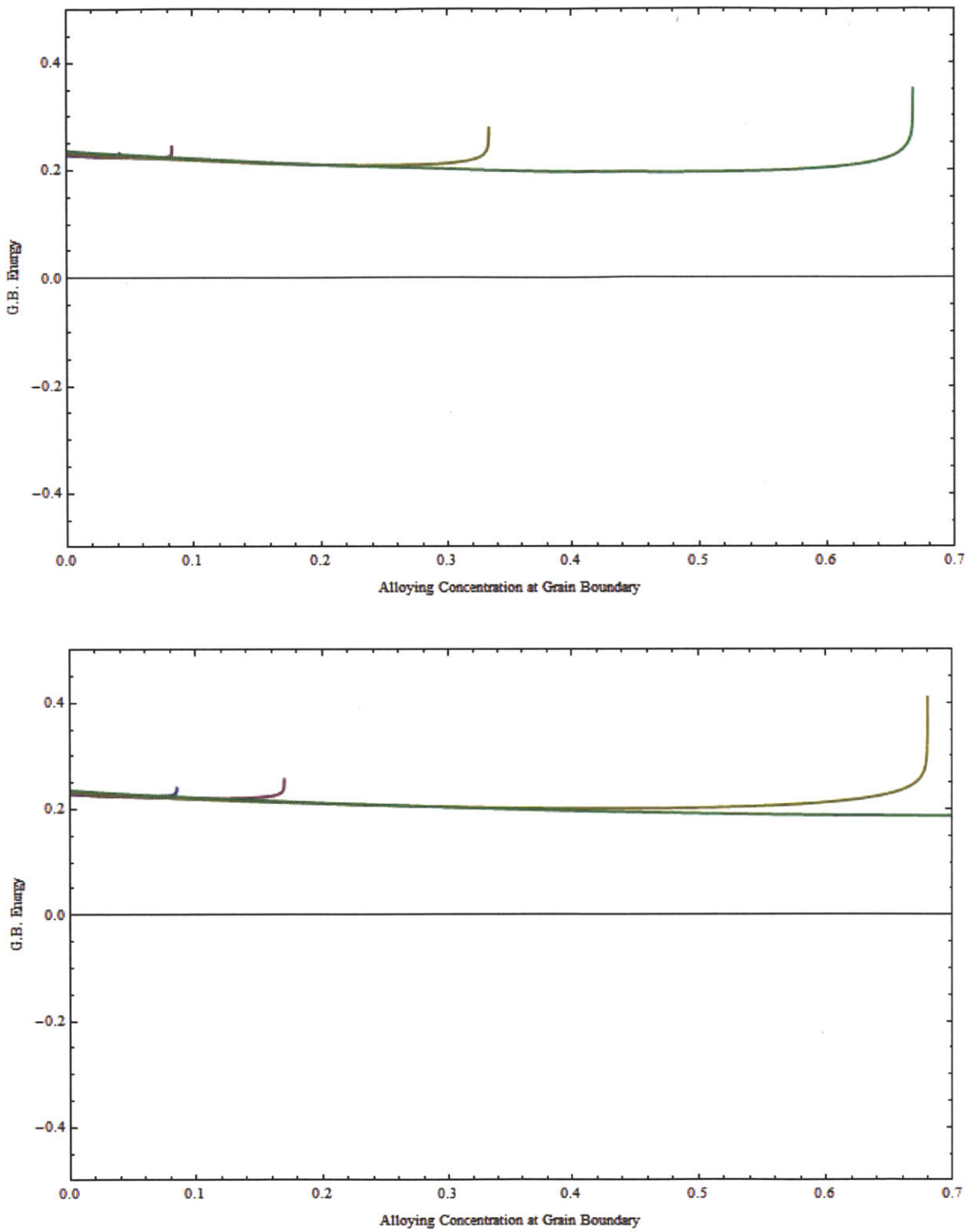

Figure8: Grain Boundary energies in eV/ atom versus Grain Boundary Composition for TaW samples. Blue:Ta0.5at%W,Purple:Ta1at%W,Yellow:Ta4at%W,Green:Ta8at%W. Top: D=12. Bottom: D=25.

3.2 Work of fracture Data

In addition to stability, strength characteristics were also measured for the set of alloys studied. Below is a table which lists the alloys studied and their predicted work of fracture values using equation 8. Tables are organized by alloy material, and global alloying material composition. Some samples have multiple grain boundary minimization energy values, which translates to multiple work of fracture minimization values.

Global Composition of Solute	Local Composition Zn		Local Composition Bi	NiZn	CuBi
0.5%	X		X	X	X
1%	X		X	X	X
4%	X		11.3%	X	$1.01 \frac{J}{m^2}$
8%	40.6%	64.4%	10.7%	$1.13 \frac{J}{m^2}$	$1.13 \frac{J}{m^2}$

Table 5: Work of fracture data based on global composition for various alloys which demonstrate grain boundary segregation. Grains are taken to be 12 nm in length.

Global Composition of Solute	Local Composition Zn		Local Composition Bi	NiZn	CuBi
0.5%	X		X	X	X
1%	X		11.9%	X	$1.00\frac{J}{m^2}$
4%	40.2%	64.5%	11.1%	$1.01\frac{J}{m^2}$	$1.01\frac{J}{m^2}$
8%	45.6%		10.7%	$1.13\frac{J}{m^2}$	$1.13\frac{J}{m^2}$

Table 6: Work of fracture data based on global composition for various alloys which demonstrate grain boundary segregation. Grains are taken to be 25 nm in length.

These values are of a reasonable magnitude, and will later be compared to bulk samples to determine when nanocrystalline alloys might be better suited for certain types of applications. As mentioned before, some alloys have multiple local compositions for zero grain boundary energy, and this is represented in the tables above by a split in the local alloying material composition.

Discussion on Outcomes of Simulation

4.1 Stability in Nanocrystalline Alloys

Within the materials studied, the alloys were separated so as to group them up according to energy values for heat of segregation energies and Heat of mixing. Table 3 shows data arranged by segregation energy, while table 4 shows data arranged for mixing energy. Referring back to the previous section, it is seen that of the alloys studied, CuBi and NiZn show preference towards segregation within the confines of the RNS model and the assumptions made in this study. Conversely, FeCr, FeZn, NiCu, NiPb, and TaW all show no tendency to segregate. Table 7 and table 8 below group these materials together, again illustrating their energy values for segregation and mixing.

	Positive Heat of Segregation	Heat of Mixing		**Negative Heat of Segregation**	Heat of Mixing
CuBi	$96000\ \frac{J}{m^2}$	$78100\ \frac{J}{m^2}$			
NiZn	$23400\ \frac{J}{m^2}$	$56900\ \frac{J}{m^2}$			

Table 7: Alloys exhibiting segregation tendencies in nanocrystalline structures.

	Positive Heat of Segregation	Heat of Mixing		**Negative Heat of Segregation**	Heat of Mixing
TaW	$13200\frac{J}{m^2}$	$20500\frac{J}{m^2}$	**FeZn**	$-20000\frac{J}{m^2}$	$10600\frac{J}{m^2}$
NiPb	$10700\frac{J}{m^2}$	$59000\frac{J}{m^2}$	**NiCu**	$-7690\frac{J}{m^2}$	$14000\frac{J}{m^2}$
			FeCr	$-1680\frac{J}{m^2}$	$-5\,920\frac{J}{m^2}$

Table 8: Alloys not exhibiting segregation tendencies in nanocrystalline structures.

Looking at these tables, it can be seen that those alloys with larger energy values are most likely to display segregation. This applies mostly to segregation energies, but also appears to hold for mixing energies. And while this might universal, it does stand when taking the RNS model into consideration, as well as the associated assumptions that go with it.

Knowing which alloys do and do not segregate can help determine which metals will show stability in a nanocrystalline form. Using the equations above, it is shown that minimizing the magnitude of segregation energy results in an overall minimization of free energy. This leads to a more stable configuration, and thus points towards stability. Taking those alloys which demonstrated segregation tendencies; CuBi and NiZn, it can be said that these alloys will likely show nanocrystalline stability. However, this stability is dependent upon following those assumptions made by the RNS model. The most important of these assumptions for this study is the tendency to segregate, either majority or minority alloying metal, towards the grain boundary. While calculations made in this work show these

samples to exhibit segregation tendencies, segregation is not necessarily guaranteed. However, when reviewing the literature, it was found that CuBi shows a tendency to segregate in bulk material (Alber, Müllejans and Rühle). This result is favorable, showing that the RNS model could predict segregation in nanocrystalline metal alloys.

4.2 Comparative Analysis of Nanocrystalline Alloys and Bulk Counterparts

Material work of fracture data was collected for CuBi and NiZn alloys (Murr). The work of fracture is not necessarily the most reliable measure of a material's failure strength. It is however a good relative measure of how much energy one material requires to fracture vs. another. Below is a table which represents some bulk work of fracture values for CuBi and NiZn. Values were calculated using a simple model of constituent proportions, as in the case with the work of fracture for nanocrystalline alloys.

NiZn	CuBi
$.155\frac{J}{m^2}$	$.150\frac{J}{m^2}$
$.136\frac{J}{m^2}$	$.5\frac{J}{m^2}$
$.138\frac{J}{m^2}$	$1\frac{J}{m^2}$
$.219\frac{J}{m^2}$	

*Table 9: Bulk Work of fracture values for CuBi and NiZn (*Murr)

These values are considered average for the materials in question. Values for Copper-Bismuth were estimated given a range of reasonable values. *Figure 9* shows how bulk and nanocrystalline work of fracture values compare. The line through the center of graph represents a unity in terms of nanocrystalline values.

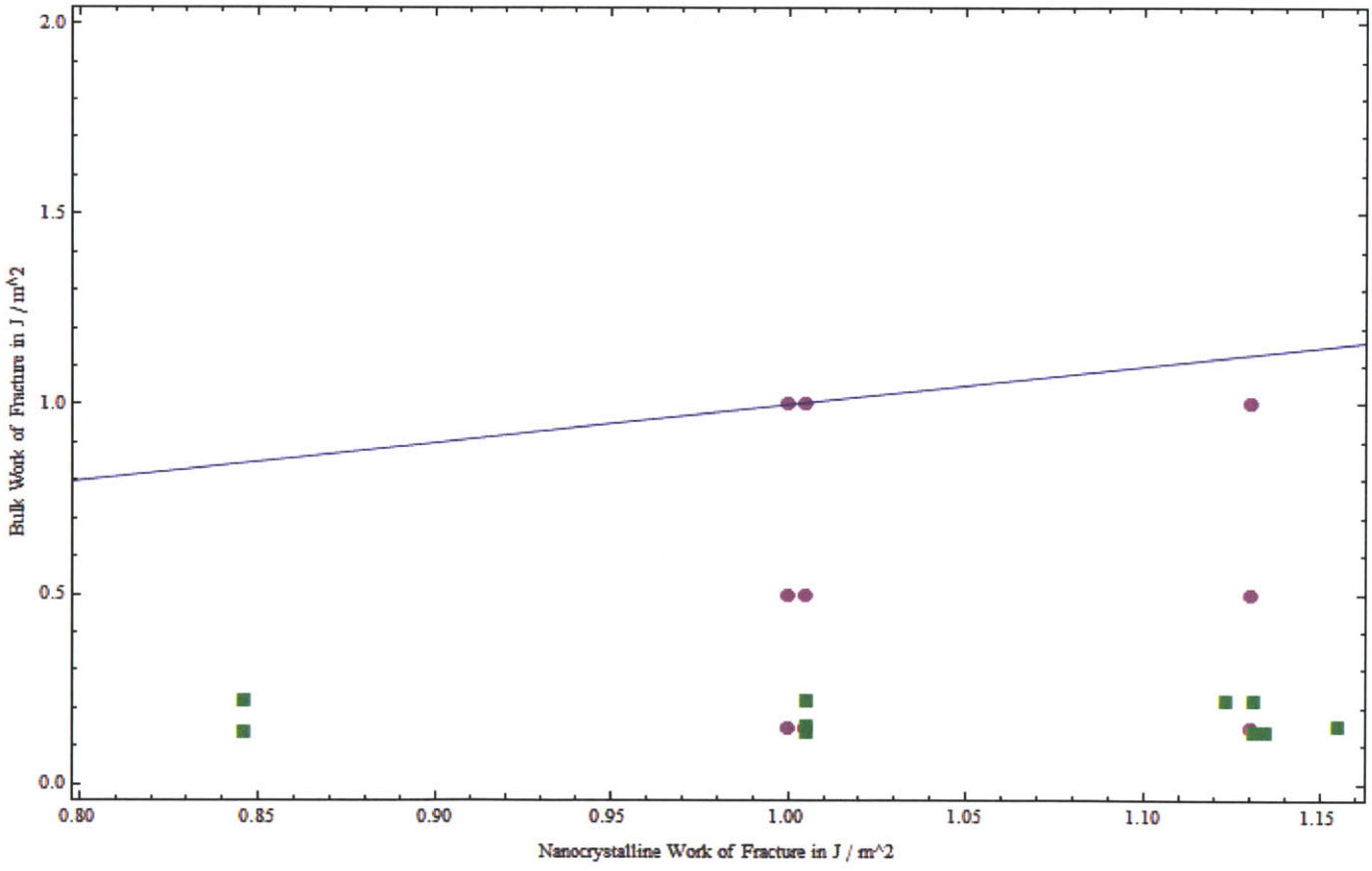

Figure 9: A representation of nanocrystalline work of fracture energy vs. bulk work of fracture energy for CuBi(Pink) and NiZn(Green).

Bulk values above represent materials which can store more energy, while those below show materials which store less energy.

The graph above shows how for a given alloy, a nanocrystalline material will require more energy to fracture than a bulk material. Nanocrystalline metals are then better suited for applications in which a higher energy to fracture is needed. This falls in line with conventional knowledge of nanocrystalline metals, and is a good result to find based on data gathered from the RNS model.

4.3 Future Work with Nanoscale Metal Alloys

Future work that can be done will involve using more accurate equations for calculating surface energy and work of fracture values. As was mentioned before, a simplistic surface energy model was used in order to observe trends and model material behavior. More accurate values could be found or calculated. In addition, work of fracture values were calculated using a bulk model which assumes segregation will not arise within grain structures. This was done, as with surface energy, to find order of magnitude data which could be quickly and easily compared for the purpose of finding basic tendencies. Fine tuning an equation which more appropriately takes RNS assumptions into consideration will allow the calculation of values to higher orders.

Further work which can be done in this area will involve testing results based on theories asserted in this work. Based on the RNS model, XRD analysis can show whether grains of the size and composition can be made of those alloys considered stable. Additionally, tests can be done to show instability in those alloys which do

not display segregation tendencies. Again though, the RNS model can only predict stability or a lack of in models which fulfill the criteria of segregation of either alloying constituent towards the grain boundaries. Should this condition not hold within the material being analyzed, the RNS model is unable to accurately predict stability. A second set of experiments that could be utilized in future work are mechanical strength tests. These tests would show the validity of the work of fracture data calculated for the bulk and nanocrystalline alloys, and show which materials are ideal for different uses. These are likely to be inconsistent with calculated values to some extent due to the simplistic nature in which work of fracture was determined. However, the trends which both sets of data follow should be similar.

Conclusion

Nanocrystalline metal alloys are capable of achieving materials characteristics that their bulk counterparts are not. In this study, it was shown how a regular nanocrystalline solution model can accurately describe the stability of nanocrystalline alloys. A series of metals were studied, and values were attained for energy terms, calculated using RNS. It was determined that segregation, and therefore stability, is seen in both CuBi and NiZn alloys. *Figures 2, 7* show this behavior. These alloys were then analyzed in terms of their fracture characteristics, and compared with their bulk counterparts. As seen in *figure 9*, nanocrystalline CuBi and NiZn both require more energy to fracture than in bulk material. The data which results from this work, while not held to the highest level of precision, is useful in showing trends, and predicting behavior of metal alloys using the RNS model. Further work can be done using this study as a benchmark, and can lead to better, more accurate results.

Acknowledgements

I would like to thank Professor Chris Schuh for allowing me to work with him in his group. His mentorship, not only within this project, but with my academic career in general has been very helpful, and greatly appreciated.

I would like to thank Heather Murdoch for helping me in innumerable ways. Her guidance with this project has helped it become what is documented here, and I would not have been able to complete this work without her. Her assistance, not only in completing the thesis project, but in teaching me how to conduct research, has gone a long way in developing me as a professional.

Bibliography

Alber, U., H. Müllejans & M. Rühle (1999) Bismuth segregation at copper grain boundaries. *Acta Materialia,* 47, 4047-4060.

Fultz, B. & H. N. Frase (2000) Grain boundaries of nanocrystalline materials - their widths, compositions, and internal structures. *Hyperfine Interactions,* 130, 81-108.

Ibach, H, Sander, D (2002) 4.4 Surface free energy and surface stress. Landolt-Börnstein - Group III Condensed Matter Numerical Data and Functional Relationships in Science and Technology, 19-44.

Murr, L.E. (1975) Interfacial phenomena in metals and alloys. Addison-Wesley Publishing Company Advanced Book Program 130-131.

Trelewicz, J. R. & C. A. Schuh (2009) Grain boundary segregation and thermodynamically stable binary nanocrystalline alloys. *Physical Review B,* 79, 13.

Weissmuller, J. (1993) ALLOY EFFECTS IN NANOSTRUCTURES. *Nanostructured Materials,* 3, 261-272.